

Measurement of the cross section for hard exclusive π^0 leptonproduction

COMPASS Collaboration

M. G. Alexeev^y, G. D. Alexeev^g, A. Amoroso^{y,z}, V. Andrieux^{i,ab}, N. V. Anfimov^g, V. Anosov^g, A. Antoshkin^g, K. Augsten^{g,r}, W. Augustyniak^{ac}, C. D. R. Azevedo^a, B. Badełek^{ad}, F. Balestra^{y,z}, M. Ball^c, J. Barth^c, R. Beck^c, Y. Bedfer^t, J. Bernhard^{l,i}, M. Bodlak^q, P. Bordalo^{k,1}, F. Bradamante^{w,x}, A. Bressan^{w,x}, M. Büchele^h, V. E. Burtsev^{aa}, W.-C. Chang^u, C. Chatterjee^f, M. Chiosso^{y,z}, A. G. Chumakov^{aa}, S.-U. Chung^{o,2,3}, A. Cicuttin^{x,4}, M. L. Crespo^{x,4}, S. Dalla Torre^x, S. S. Dasgupta^f, S. Dasgupta^{w,x}, O. Yu. Denisov^{z,*}, L. Dhara^f, S. V. Donskov^s, N. Doshita^{af}, Ch. Dreisbach^o, W. Dünneweber⁵, R. R. Dusaev^{aa}, A. Efremov^g, P. D. Eversheim^c, M. Faessler⁵, A. Ferrero^t, M. Finger^q, M. Finger jr.^q, H. Fischer^h, C. Franco^k, N. du Fresne von Hohenesche^{l,i}, J. M. Friedrich^{o,*}, V. Frolov^{g,i}, E. Fuchey^t, F. Gautheron^{b,ab}, O. P. Gavrichtchouk^g, S. Gerassimov^{n,o}, J. Giarra^l, I. Gnesi^{y,z}, M. Gorzellik^{h,6}, A. Grasso^{y,z}, A. Gridin^g, M. Grosse Perdekamp^{ab}, B. Grube^o, A. Guskov^g, D. Hahne^d, G. Hamar^x, D. von Harrach^l, R. Heitz^{ab}, F. Herrmann^h, N. Horikawa^{p,7}, N. d'Hose^t, C.-Y. Hsieh^{u,8}, S. Huber^o, S. Ishimoto^{af,9}, A. Ivanov^{y,z}, T. Iwata^{af}, M. Jandek^r, V. Jary^r, R. Joosten^c, P. Jörg^{h,10}, K. Juraskova^r, E. Kabuß^l, F. Kaspar^o, A. Kerbizi^{w,x}, B. Ketzer^c, G. V. Khaustov^s, Yu. A. Khokhlov^{s,11}, Yu. Kisselev^g, F. Klein^d, J. H. Koivuniemi^{b,ab}, V. N. Kolosov^s, K. Kondo Horikawa^{af}, I. Konorov^{n,o}, V. F. Konstantinov^s, A. M. Kotzinian^{z,12}, O. M. Kouznetsov^g, Z. Kral^q, M. Krämer^o, F. Krinner^o, Z. V. Kroumchtein^{g,29}, Y. Kulinich^{ab}, F. Kunne^t, K. Kurek^{ac}, R. P. Kurjata^{ae}, A. Kveton^r, S. Levorato^x, Y.-S. Lian^{u,13}, J. Lichtenstadt^v, P.-J. Lin^t, R. Longo^{ab}, V. E. Lyubovitskij^{aa,14}, A. Maggiora^z, A. Magnon^{ab,28}, N. Makins^{ab}, N. Makke^{x,4}, G. K. Mallotⁱ, S. A. Mamon^{aa}, B. Marianski^{ac}, A. Martin^{w,x}, J. Marzec^{ae}, J. Matoušek^{w,x,q}, T. Matsuda^m, G. V. Meshcheryakov^g, M. Meyer^{ab,t}, W. Meyer^b, Yu. V. Mikhailov^s, M. Mikhasenko^c, E. Mitrofanov^g, N. Mitrofanov^g, Y. Miyachi^{af}, A. Moretti^{w,x}, C. Naim^t, A. Nagaytsev^g, D. Neyret^t, J. Nový^{r,i}, W.-D. Nowak^l, G. Nukazuka^{af}, A. S. Nunes^k, A. G. Olshevsky^g, M. Ostrick^l, D. Panzieri^{z,15}, B. Parsamyan^{y,z},

*Corresponding authors

Email addresses: oleg.denisov@cern.ch (O. Yu. Denisov), jan.friedrich@cern.ch (J. M. Friedrich)

¹Also at Instituto Superior Técnico, Universidade de Lisboa, Lisbon, Portugal

²Also at Dept. of Physics, Pusan National University, Busan 609-735, Republic of Korea

³Also at at Physics Dept., Brookhaven National Laboratory, Upton, NY 11973, USA

⁴Also at Abdus Salam ICTP, 34151 Trieste, Italy

⁵Supported by the DFG cluster of excellence 'Origin and Structure of the Universe' (www.universe-cluster.de) (Germany)

⁶Supported by the DFG Research Training Group Programmes 1102 and 2044 (Germany)

⁷Also at Chubu University, Kasugai, Aichi 487-8501, Japan

⁸Also at Dept. of Physics, National Central University, 300 Jhongda Road, Jhongli 32001, Taiwan

⁹Also at KEK, 1-1 Oho, Tsukuba, Ibaraki 305-0801, Japan

¹⁰Present address: Universität Bonn, Physikalisches Institut, 53115 Bonn, Germany

¹¹Also at Moscow Institute of Physics and Technology, Moscow Region, 141700, Russia

¹²Also at Yerevan Physics Institute, Alikhanian Br. Street, Yerevan, Armenia, 0036

¹³Also at Dept. of Physics, National Kaohsiung Normal University, Kaohsiung County 824, Taiwan

¹⁴Also at Institut für Theoretische Physik, Universität Tübingen, 72076 Tübingen, Germany

¹⁵Also at University of Eastern Piedmont, 15100 Alessandria, Italy

¹⁶Present address: RWTH Aachen University, III. Physikalisches Institut, 52056 Aachen, Germany

¹⁷Supported by BMBF - Bundesministerium für Bildung und Forschung (Germany)

¹⁸Supported by FP7, HadronPhysics3, Grant 283286 (European Union)

¹⁹Supported by MEYS, Grant LM20150581 (Czech Republic)

²⁰Supported by B.Sen fund (India)

²¹Supported by FCT, COMPETE and QREN, Grants CERN/FP 116376/2010, 123600/2011 and CERN/FIS-NUC/0017/2015 (Portugal)

²²Supported by MEXT and JSPS, Grants 18002006, 20540299, 18540281 and 26247032, the Daiko and Yamada Foundations (Japan)

²³Supported by the Ministry of Science and Technology (Taiwan)

²⁴Supported by the Israel Academy of Sciences and Humanities (Israel)

²⁵Supported by the Russian Federation program "Nauka" (Contract No. 0.1764.GZB.2017) (Russia)

²⁶Supported by the National Science Foundation, Grant no. PHY-1506416 (USA)

²⁷Supported by NCN, Grant 2017/26/M/ST2/00498 (Poland)

²⁸Retired

²⁹Deceased

arXiv:1903.12030v1 [hep-ex] 28 Mar 2019

S. Paul^o, J.-C. Peng^{ab}, F. Pereira^a, M. Pešek^q, D. V. Peshekhonov^g, M. Pešková^q, N. Pierre^{h,t}, S. Platchkov^t, J. Pochodzalla^l, V. A. Polyakov^s, J. Pretz^{d,16}, M. Quaresima^u, C. Quintans^k, S. Ramos^{k,1}, C. Regali^h, G. Reicherz^b, C. Riedl^{ab}, D. I. Ryabchikov^{s,o}, A. Rybnikov^g, A. Rychter^{ae}, V. D. Samoylenko^s, A. Sandacz^{ac}, S. Sarkar^f, I. A. Savin^g, G. Sbrizzai^{w,x}, H. Schmieden^d, A. Selyunin^g, L. Silva^k, L. Sinha^f, M. Slunecka^g, J. Smolik^g, A. Srnka^e, D. Steffen^{i,o}, M. Stolarski^k, O. Subrt^{i,r}, M. Sulc^j, H. Suzuki^{af,7}, A. Szabelski^{w,x,ac}, T. Szameitat^{h,6}, P. Sznajder^{ac}, S. Tessaro^x, F. Tessarotto^x, A. Thiel^c, J. Tomsa^q, F. Tosello^z, V. Tskhayⁿ, S. Uhl^o, B. I. Vasilishin^{aa}, A. Vauth^{d,i}, B. M. Veit^{l,i}, J. Veloso^a, A. Vidon^t, M. Virius^f, M. Wagner^c, S. Wallner^o, M. Wilfert^l, K. Zaremba^{ae}, P. Zavada^g, M. Zavertyaevⁿ, E. Zemlyanichkina^g, Y. Zhao^x, M. Ziembicki^{ae}

^aUniversity of Aveiro, I3N - Physics Department, 3810-193 Aveiro, Portugal

^bUniversität Bochum, Institut für Experimentalphysik, 44780 Bochum, Germany

^cUniversität Bonn, Helmholtz-Institut für Strahlen- und Kernphysik, 53115 Bonn, Germany

^dUniversität Bonn, Physikalisches Institut, 53115 Bonn, Germany

^eInstitute of Scientific Instruments of the CAS, 61264 Brno, Czech Republic

^fMatrivani Institute of Experimental Research & Education, Calcutta-700 030, India

^gJoint Institute for Nuclear Research, 141980 Dubna, Moscow region, Russia

^hUniversität Freiburg, Physikalisches Institut, 79104 Freiburg, Germany

ⁱCERN, 1211 Geneva 23, Switzerland

^jTechnical University in Liberec, 46117 Liberec, Czech Republic

^kLIP, 1649-003 Lisbon, Portugal

^lUniversität Mainz, Institut für Kernphysik, 55099 Mainz, Germany

^mUniversity of Miyazaki, Miyazaki 889-2192, Japan

ⁿLebedev Physical Institute, 119991 Moscow, Russia

^oTechnische Universität München, Physik Dept., 85748 Garching, Germany

^pNagoya University, 464 Nagoya, Japan

^qCharles University in Prague, Faculty of Mathematics and Physics, 12116 Prague, Czech Republic

^rCzech Technical University in Prague, 16636 Prague, Czech Republic

^sState Scientific Center Institute for High Energy Physics of National Research Center 'Kurchatov Institute', 142281 Protvino, Russia

^tIRFU, CEA, Université Paris-Saclay, 91191 Gif-sur-Yvette, France

^uAcademia Sinica, Institute of Physics, Taipei 11529, Taiwan

^vTel Aviv University, School of Physics and Astronomy, 69978 Tel Aviv, Israel

^wUniversity of Trieste, Dept. of Physics, 34127 Trieste, Italy

^xTrieste Section of INFN, 34127 Trieste, Italy

^yUniversity of Turin, Dept. of Physics, 10125 Turin, Italy

^zTorino Section of INFN, 10125 Turin, Italy

^{aa}Tomsk Polytechnic University, 634050 Tomsk, Russia

^{ab}University of Illinois at Urbana-Champaign, Dept. of Physics, Urbana, IL 61801-3080, USA

^{ac}National Centre for Nuclear Research, 00-681 Warsaw, Poland

^{ad}University of Warsaw, Faculty of Physics, 02-093 Warsaw, Poland

^{ae}Warsaw University of Technology, Institute of Radioelectronics, 00-665 Warsaw, Poland

^{af}Yamagata University, Yamagata 992-8510, Japan

Abstract

We report on a measurement of hard exclusive π^0 muoproduction on the proton by COMPASS using 160 GeV/c polarised μ^+ and μ^- beams of the CERN SPS impinging on a liquid hydrogen target. From the average of the measured μ^+ and μ^- cross sections, the virtual-photon proton cross section is determined as a function of the squared four-momentum transfer between initial and final proton in the range $0.08 (\text{GeV}/c)^2 < |t| < 0.64 (\text{GeV}/c)^2$. The average kinematics of the measurement are $\langle Q^2 \rangle = 2.0 (\text{GeV}/c)^2$, $\langle \nu \rangle = 12.8 \text{ GeV}$, $\langle x_{Bj} \rangle = 0.093$ and $\langle -t \rangle = 0.256 (\text{GeV}/c)^2$. Fitting the azimuthal dependence reveals a combined contribution by transversely and longitudinally polarised photons of $(8.1 \pm 0.9_{\text{stat}} \pm 1.1_{\text{sys}}) \text{ nb}/(\text{GeV}/c)^2$, as well as transverse-transverse and longitudinal-transverse interference contributions of $(-6.0 \pm 1.3_{\text{stat}} \pm 0.7_{\text{sys}}) \text{ nb}/(\text{GeV}/c)^2$ and $(1.4 \pm 0.5_{\text{stat}} \pm 0.3_{\text{sys}}) \text{ nb}/(\text{GeV}/c)^2$, respectively. Our results provide important input for modelling Generalised Parton Distributions. In the context of the phenomenological Goloskokov-Kroll model, the statistically significant transverse-transverse interference contribution constitutes clear experimental evidence for the chiral-odd GPD \bar{E}_T .

Keywords: Quantum chromodynamics, muoproduction, hard exclusive meson production, Generalised Parton Distributions, COMPASS

1. Introduction

Measurements of pseudoscalar mesons produced in hard exclusive lepton-nucleon scattering provide important data for phenomenological parameterisations of Generalised Parton Distributions (GPDs) [1–5]. In the past two decades, GPDs have shown to be a very rich and useful construct for both experiment and theory as their determination allows for a detailed description of the parton structure of the nucleon. In particular, GPDs correlate transverse spatial positions and longitudinal momentum fractions of the partons in the nucleon. They embed parton distribution functions and nucleon form factors, and they give access to energy-momentum-tensor form factors. For each quark flavour, there exist four parton-helicity-conserving (chiral-even) GPDs, denoted H , \tilde{H} , E , and \tilde{E} , and four parton-helicity-flip (chiral-odd) GPDs, denoted H_T , \tilde{H}_T , E_T , and \tilde{E}_T . While hard production of vector mesons is sensitive primarily to the GPDs H and E , the production of pseudoscalar mesons by longitudinally polarised virtual photons is sensitive to \tilde{H} and \tilde{E} in the leading-twist description.

Contributions from transversely polarised virtual photons to the production of spin-0 mesons are expected to be suppressed in the production amplitude by $1/Q$ [6], where Q^2 is the virtuality of the photon γ^* that is exchanged between muon and proton. However, experimental data on exclusive π^+ production from HERMES [7] and on exclusive π^0 production from JLab CLAS [8–11] and Hall A [12–14] suggest that such contributions are substantial. In the GPD formalism such contributions are possible if a quark helicity-flip GPD couples to a twist-3 wave function [15, 16]. In the framework of the phenomenological model of Ref. [15], pseudoscalar-meson production is described by the GPDs \tilde{H} , \tilde{E} , H_T and $\tilde{E}_T = 2\tilde{H}_T + E_T$. Different sensitivities to these GPDs are expected when comparing π^+ vs. π^0 production. When taking into account the relative signs and sizes of these GPDs for u and d quarks, the different quark flavour contents of these mesons lead to different predictions for the $|t|$ -dependence of the cross section, especially at small values of $|t|$. Here, t is the square of the four-momentum transfer between initial and final nucleon. The production of π^+ mesons is dominated by the contributions from longitudinally polarised virtual photons, of which a major part originates from pion-pole exchange that is the main contributor to \tilde{E} . Also the contributions from \tilde{H} and H_T are significant, and there is a strong cancellation between the contributions from \tilde{E}_T for u and d quarks. On the contrary, in the case of π^0 production there is no pion-pole exchange, the contributions from \tilde{H} and H_T are small and a large contribution from transversely polarised photons is generated mainly by \tilde{E}_T .

These differences between π^+ and π^0 production are experimentally supported. While for π^+ production a fast decrease of the cross section with increasing $|t|$ is predicted by theoretical models and confirmed by the experimental

results from HERMES [7], for π^0 production a dip is expected as $|t| \rightarrow 0$ [15] and confirmed by results in the JLab kinematic domain [9, 10, 13]. Constraints for modelling the poorly known GPD \tilde{E}_T were obtained in a lattice-QCD study [17] of its moments. The COMPASS results on exclusive π^0 production in muon-proton scattering presented in this Letter provide new input for modelling this GPD and chiral-odd (‘transversity’) GPDs in general.

2. Formalism

The reduced cross section for hard exclusive meson production by scattering a polarised lepton beam off an unpolarised proton target reads:

$$\frac{d^2\sigma_{\gamma^*p}^{\leftrightarrow}}{dtd\phi} = \frac{1}{2\pi} \left[\frac{d\sigma_T}{dt} + \epsilon \frac{d\sigma_L}{dt} + \epsilon \cos(2\phi) \frac{d\sigma_{TT}}{dt} + \sqrt{2\epsilon(1+\epsilon)} \cos\phi \frac{d\sigma_{LT}}{dt} \mp |P_l| \sqrt{2\epsilon(1-\epsilon)} \sin\phi \frac{d\sigma'_{LT}}{dt} \right], \quad (1)$$

where the sign \mp of the lepton beam polarisation P_l corresponds to negative and positive helicity of the incoming lepton, respectively, denoted by \leftrightarrow . The conversion from the lepton-nucleon cross section to the virtual-photon nucleon cross section, using the one-photon-exchange approximation, is explained in Sect. 5. The contribution to the cross section from transversely (longitudinally) polarised virtual photons is denoted by σ_T (σ_L). The symbols σ_{TT} and $\sigma_{LT}, \sigma'_{LT}$ denote contributions from the interference between transversely and longitudinally polarised virtual photons, respectively, with transversely polarised ones. The factor

$$\epsilon = \frac{1 - y - \frac{y^2\gamma^2}{4}}{1 - y + \frac{y^2}{2} + \frac{y^2\gamma^2}{4}} \quad (2)$$

is the virtual-photon polarisation parameter and ϕ is the azimuthal angle between the lepton scattering plane and the hadron production plane, see Fig. 1. Here, $Q^2 = -(k_\mu - k_{\mu'})^2$ is the photon virtuality, $\nu = (k_\mu^0 - k_{\mu'}^0)$ the energy of the virtual photon in the target rest frame, $y = \nu/k_\mu^0$ and $\gamma^2 = Q^2/\nu^2$, where k_μ and $k_{\mu'}$ denote the four-momenta of the incoming and the scattered muon in the laboratory system, respectively.

The spin-independent cross section can be obtained by averaging the two spin-dependent cross sections,

$$\frac{d^2\sigma_{\gamma^*p}}{dtd\phi} = \frac{1}{2} \left(\frac{d^2\sigma_{\gamma^*p}^{\leftarrow}}{dtd\phi} + \frac{d^2\sigma_{\gamma^*p}^{\rightarrow}}{dtd\phi} \right). \quad (3)$$

When forming this average, the last term in Eq. (1) cancels if the magnitude $|P_l|$ of the beam polarisation is the same for measurements with μ^+ and μ^- beam, so that

$$\frac{d^2\sigma_{\gamma^*p}}{dtd\phi} = \frac{1}{2\pi} \left[\frac{d\sigma_T}{dt} + \epsilon \frac{d\sigma_L}{dt} + \epsilon \cos(2\phi) \frac{d\sigma_{TT}}{dt} + \sqrt{2\epsilon(1+\epsilon)} \cos(\phi) \frac{d\sigma_{LT}}{dt} \right]. \quad (4)$$

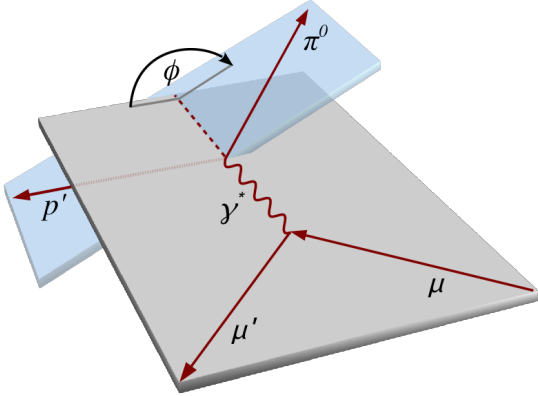


Figure 1: Definition of ϕ , the azimuthal angle between the lepton-scattering and π^0 -production planes.

The individual contributions appearing in Eq. (4) are related to convolutions of GPDs and meson distribution amplitudes with individual hard scattering amplitudes [10, 15]:

$$\frac{d\sigma_T}{dt} \propto \left[(1 - \xi^2) |\langle H_T \rangle|^2 - \frac{t'}{8M^2} |\langle \bar{E}_T \rangle|^2 \right], \quad (5)$$

$$\frac{d\sigma_L}{dt} \propto \left[(1 - \xi^2) |\langle \tilde{H} \rangle|^2 - 2\xi^2 \text{Re} \left[\langle \tilde{H} \rangle^* \langle \tilde{E} \rangle \right] - \frac{t'}{4M^2} \xi^2 |\langle \tilde{E} \rangle|^2 \right], \quad (6)$$

$$\frac{d\sigma_{TT}}{dt} \propto t' |\langle \bar{E}_T \rangle|^2, \quad (7)$$

$$\frac{d\sigma_{LT}}{dt} \propto \xi \sqrt{1 - \xi^2} \sqrt{-t'} \text{Re} \left[\langle H_T \rangle^* \langle \tilde{E} \rangle \right]. \quad (8)$$

Here, the aforementioned convolutions are denoted by triangular brackets, $t' = t - t_{min}$ with $|t_{min}|$ being the kinematically smallest possible value of $|t|$, and M is the mass of the proton. The quantity ξ is equal to one half of the longitudinal momentum fraction transferred between the initial and final proton and can be approximated at COMPASS kinematics as

$$\xi \approx \frac{x_{Bj}}{2 - x_{Bj}}, \quad (9)$$

where $x_{Bj} = Q^2/(2M\nu)$.

3. Experimental set-up and data selection

The main component of the COMPASS set-up is the two-stage magnetic spectrometer. Each spectrometer stage comprises a dipole magnet complemented by a variety of tracking detectors, a muon filter for muon identification and an electromagnetic (ECal) as well as a hadron calorimeter. A detailed description of the set-up can be found in Refs. [18–20].

The data used for this analysis were collected within four weeks in 2012, during which the COMPASS spectrometer was complemented by a 2.5 m long liquid-hydrogen

target surrounded by a time-of-flight (TOF) system, and a third electromagnetic calorimeter that was placed directly downstream of the target. The TOF detector consisted of two cylinders, each made of 24 scintillating-counter slats, mounted concentrically around the target.

In order to determine the spin-independent cross section through Eq. (3), data with μ^+ and μ^- beam were taken separately. The natural polarisation of the muon beam provided by the CERN SPS originates from the parity-violating decay in flight of the parent meson, which implies opposite polarisation for μ^+ and μ^- beams. Within regular time intervals during the measurement, charge and polarisation of the muon beam were swapped simultaneously. In total, a luminosity of 18.9 pb^{-1} was collected for the μ^+ beam with negative polarisation and 23.5 pb^{-1} for the μ^- beam with positive polarisation. For both beams, the absolute value of the average beam polarisation is about 0.8 with an uncertainty of about 0.04.

In the data analysis, π^0 mesons are selected by their dominant two-photon decay. At least two neutral clusters are required that had to be detected above the respective threshold in one of the electromagnetic calorimeters, in conjunction with an interaction vertex reconstructed within the target using the incoming and outgoing muon tracks. The outgoing muon is identified by requiring that it has the same charge as the beam particle and traverses more than 15 radiation lengths. As neutral cluster we denote a reconstructed calorimeter cluster that is not associated to a charged track, thereby including any cluster in case of the most upstream calorimeter that had no tracking system in front.

For each interaction vertex and each combination of two neutral clusters, the kinematics of the recoil proton are predicted from the four-momentum balance of the analysed process, $\mu p \rightarrow \mu' p' \pi^0$, $\pi^0 \rightarrow \gamma\gamma$, by using the reconstructed spectrometer information, i.e. the vertex position, the momenta of the incoming and outgoing muons as well as the energy and position of the two clusters. The predicted properties of the recoil proton p' are compared to the properties of each track candidate as reconstructed by the TOF system. Note that the four-momentum of the recoil proton is determined by the target TOF system based on the assumption that the reconstructed track belongs to a proton. Figure 2 shows an example for the result of such a comparison, including also the corresponding constraints applied for the selection of events. The Monte Carlo yields shown in this figure, denoted as HEPGEN and LEPTO, will be explained in more detail in Sect. 4.

In the case that more than one combination of vertex, cluster pair and recoil-track candidate exist that satisfy the aforementioned selection criteria for a given event, this event is excluded from the analysis. Figure 3 shows the two-photon mass distribution in the region close to the nominal π^0 mass together with the constraints applied to select π^0 mesons.

In order to further enhance the purity of the selected data and to improve the precision of the particle kin-

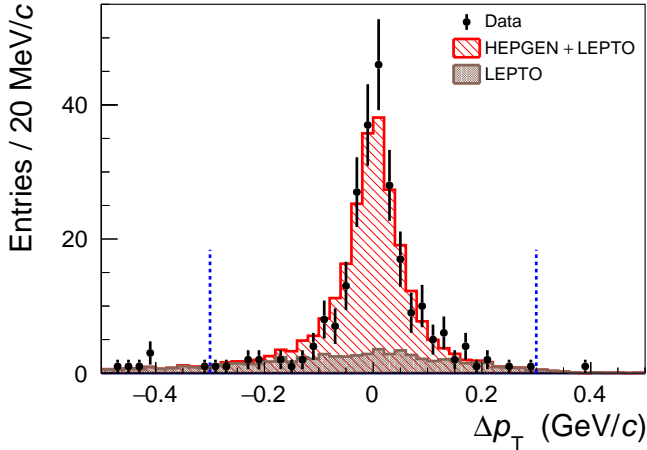


Figure 2: Measured and simulated distribution of the difference between predicted and reconstructed transverse momentum, Δp_T , of the recoil proton for the kinematic region described in the text. The vertical lines indicate the constraints applied for the selection of events. The quantity p_T is defined in the laboratory system. Error bars denote statistical uncertainties.

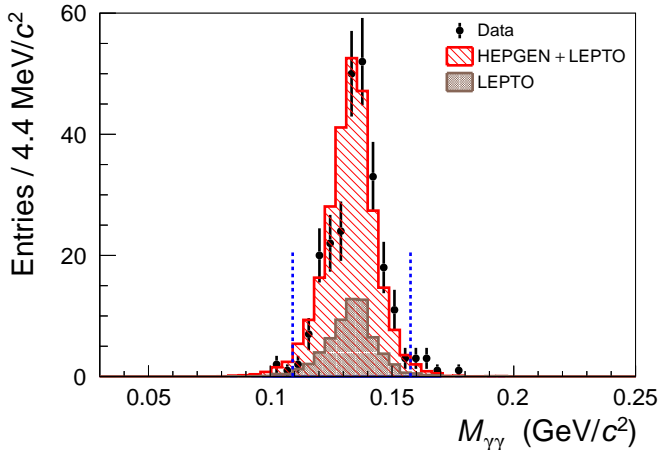


Figure 3: Distribution of the invariant mass $M_{\gamma\gamma}$ of the two-photon system. Otherwise as in figure 2.

matics at the interaction vertex, a kinematic fit for the exclusive reaction $\mu p \rightarrow \mu' p' \pi^0$ is performed, which requires a single π^0 to decay into the two photons selected as described above.

With the selection procedure described above, data are analysed in the kinematic range

$$0.08 (\text{GeV}/c)^2 < |t| < 0.64 (\text{GeV}/c)^2,$$

$$1 (\text{GeV}/c)^2 < Q^2 < 5 (\text{GeV}/c)^2$$

and $8.5 \text{ GeV} < \nu < 28 \text{ GeV}.$

In addition, two reference samples are selected in a wider kinematic range, which are denoted as signal and background sample. Apart from the extended kinematic range given below, the signal sample corresponds to the aforementioned selections. In contrast to the signal sample, the background sample contains only events with more than one combination of vertex, cluster pair and recoil-track

candidate. Apart from the small peak at zero, it contains non-exclusive events. The purpose of the reference samples is explained in the following section.

4. Estimation of the background contribution

The main background to exclusive π^0 muoproduction originates from non-exclusive deep-inelastic scattering processes. In such processes, low-energy hadrons are produced in addition to the π^0 , which remain undetected in the apparatus. In order to estimate the background contribution, two Monte Carlo generators are employed.

First, the LEPTO 6.5.1 generator with the high- p_T COMPASS tuning [21] is used to describe the non-exclusive fraction of events. Secondly, the HEPGEN++ π^0 generator is used to model the kinematics of single π^0 muoproduction [22, 23], in the following denoted by HEPGEN. The generated events from both generators are independently passed through a complete description of the COMPASS set-up [24], and the resulting simulated data are treated in the same way as it is done for real data.

As there exists essentially no information on the cross section of exclusive π^0 production in the kinematic domain of COMPASS, the two reference samples described in Sect. 3 are used to normalise the HEPGEN and LEPTO Monte Carlo yields. Using several variables, the kinematic information from beam and spectrometer measurements as well as that of the recoil-proton candidates are compared between experimental data and the two simulations in order to determine the best normalisation of each simulated data set relative to that of the experimental data. As an example of such a comparison, the undetected mass

$$M_X^2 = (k_\mu + p_p - k_{\mu'} - p_{p'} - p_{\gamma_1} - p_{\gamma_2})^2 \quad (10)$$

is shown in Fig. 4. Here, the four-momenta are denoted by p_p and $p_{p'}$ for the target and recoil proton, respectively, and by p_{γ_1} and p_{γ_2} for the two produced photons. In addition to the measured data points, the HEPGEN simulation and the sum of the HEPGEN and LEPTO simulations are shown. In order to estimate the amount of non-exclusive background, the simulated data are scaled such that they describe the data for both reference samples. The scaling factor for the LEPTO Monte Carlo yield, which is denoted by f^\pm , will be used in Sect. 5 to normalise this simulation when correcting the data for background.

The resulting fraction of non-exclusive background in the data is estimated to be $(29_{-6}^{+2}|_{\text{sys}})\%$. Here, the uncertainty is estimated by comparing the scaling factors extracted for various variables and by using several extraction methods for the scaling factors. Details are given in Ref. [25]. Contributions of other background sources are found to be negligible. For example, the production of single ω mesons, where the ω decays into a π^0 and a photon that remains undetected, was found in Monte Carlo studies to contribute at the level of 1% [25].

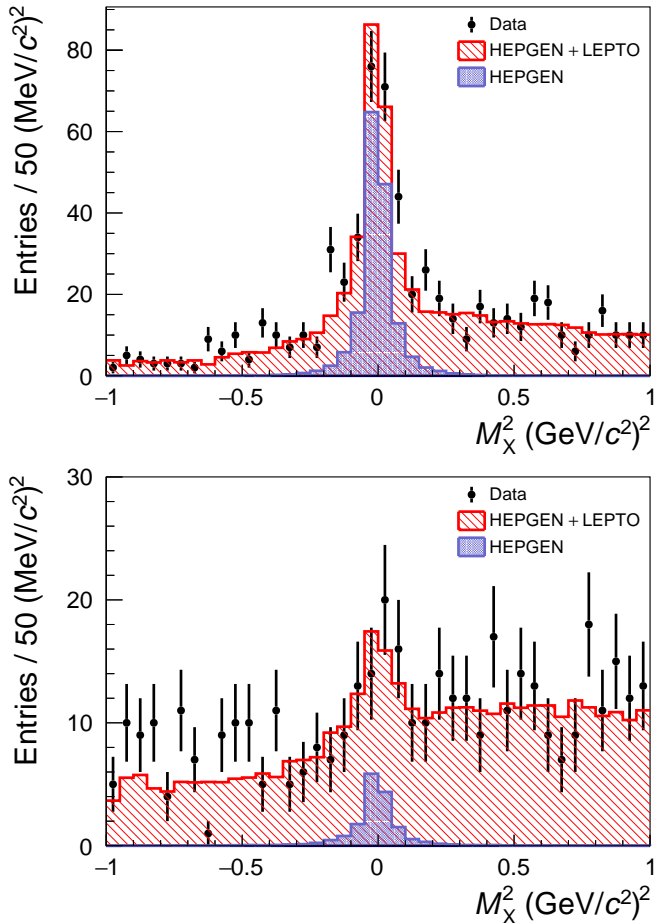


Figure 4: Distributions of the undetected mass M_X^2 for the signal (top) and background (bottom) reference samples, which are selected as described in Sect. 3 in the extended kinematic range $Q^2 > 1(\text{GeV}/c)^2$, $y > 0.05$ and $|t_{\text{TOF}}| > 0.08(\text{GeV}/c)^2$. Here, the quantities y and t_{TOF} denote the fractional energy loss of the muon and the squared four-momentum transfer to the recoil proton as measured by the target TOF system, respectively. Simulated data are also shown (see text). Note that events with the topology of exclusive π^0 production were removed from the LEPTO sample. Error bars denote statistical uncertainties.

5. Determination of the cross section

The virtual-photon proton cross section is obtained from the measured muon-proton cross section using

$$\frac{d^2\sigma}{d|t|d\phi} = \frac{1}{\Gamma(Q^2, \nu, E_\mu)} \frac{d\sigma^{\mu p}}{dQ^2 d\nu d\phi d|t|}, \quad (11)$$

where the transverse virtual-photon flux is given by

$$\Gamma(Q^2, \nu, E_\mu) = \frac{\alpha_{\text{em}}(1 - x_{\text{Bj}})}{2\pi Q^2 y E_\mu} \left[y^2 \left(1 - \frac{2m_\mu^2}{Q^2} \right) + \frac{2}{1 + Q^2/\nu^2} \left(1 - y - \frac{Q^2}{4E_\mu^2} \right) \right]. \quad (12)$$

Here, α_{em} denotes the electromagnetic fine structure constant and E_μ the zero-th component of k_μ .

For the cross section determination, the HEPGEN Monte Carlo simulation described in Sect. 4 is used. The acceptance $a(\Delta\Omega_{klmn})$ is calculated in a four-dimensional grid as the number of reconstructed events divided by the number of generated events using 8 bins in ϕ , 5 in $|t|$, 4 in Q^2 and 4 in ν . The phase-space element is given by $\Delta\Omega_{klmn} = \Delta\phi_k \Delta|t|_l \Delta Q_m^2 \Delta\nu_n$. The spacing of the grid is given in Table 1.

Table 1: Four-dimensional grid used for the calculation of the acceptance. The full width of the respective dimension is given in the bottom row of the table.

ϕ / rad	$ t $ / (GeV/c) ²	Q^2 / (GeV/c) ²	ν / GeV
$-\pi - \frac{-3\pi}{4}$	0.08 – 0.15	1 – 1.5	8.5 – 11.45
$\frac{-3\pi}{4} - \frac{-\pi}{2}$	0.15 – 0.22	1.5 – 2.24	11.45 – 15.43
.	0.22 – 0.36	2.24 – 3.34	15.43 – 0.78
.	0.36 – 0.5	3.34 – 5	20.78 – 28
.	0.5 – 0.64		
$\frac{3\pi}{4} - \pi$			
$\Delta\phi$ / rad	$\Delta t $ / (GeV/c) ²	ΔQ^2 / (GeV/c) ²	$\Delta\nu$ / GeV
2π	0.56	4	19.5

In each four-dimensional bin, the experimental yield corrected for background according to the LEPTO simulations is obtained as

$$\mathcal{Y}_{klmn}^\pm = \frac{N_{\text{data}}^{\pm, \Delta\Omega_{klmn}}}{\sum_{i=1}^{N_{\text{data}}^{\pm, \Delta\Omega_{klmn}}} \Gamma(Q_i^2, \nu_i, E_{\mu,i})} - f^\pm \frac{N_L^{\pm, \Delta\Omega_{klmn}}}{\sum_{i=1}^{N_L^{\pm, \Delta\Omega_{klmn}}} \Gamma(Q_i^2, \nu_i, E_{\mu,i})}. \quad (13)$$

Here, $N_{\text{data}}^{\pm, \Delta\Omega_{klmn}}$ is the number of measured events and $N_L^{\pm, \Delta\Omega_{klmn}}$ the number of LEPTO events within the phase-space element $\Delta\Omega_{klmn}$. The second sum represents the LEPTO simulations that are appropriately normalised by the factor f^\pm , which was introduced in Sect. 4. Each event is weighted with the transverse virtual-photon flux $\Gamma(Q_i^2, \nu_i, E_{\mu,i})$ to obtain the virtual-photon yield from the measured yields for muon-proton interactions.

The spin-dependent virtual-photon proton cross sections measured with positively or negatively charged muons are determined in each of the $(\phi_k, |t|_l)$ bins as luminosity-normalised experimental yield averaged over the measured ranges $\Delta Q^2 = 4(\text{GeV}/c)^2$ and $\Delta\nu = 19.5 \text{ GeV}$ as

$$\left\langle \frac{d^2\sigma}{d|t|d\phi} \right\rangle_{\Delta\Omega_{kl}}^\pm = \frac{1}{\mathcal{L}^\pm \Delta\Omega_{kl}} \sum_{mn} \frac{\mathcal{Y}_{klmn}^\pm}{a(\Delta\Omega_{klmn})}. \quad (14)$$

Here, $\Delta\Omega_{kl} = \Delta\phi_k \Delta|t|_l \Delta Q^2 \Delta\nu$, \mathcal{L}^\pm denotes the luminosity and $a(\Delta\Omega_{klmn})$ the acceptance in the phase-space element $\Delta\Omega_{klmn}$.

The spin-independent virtual-photon proton cross section is obtained according to Eq. (3) as average of the two

spin-dependent cross sections given in Eq. (14):

$$\left\langle \frac{d^2\sigma}{d|t|d\phi} \right\rangle_{\Delta\Omega_{kl}} = \frac{1}{2} \left(\left\langle \frac{d^2\sigma}{d|t|d\phi} \right\rangle_{\Delta\Omega_{kl}}^+ + \left\langle \frac{d^2\sigma}{d|t|d\phi} \right\rangle_{\Delta\Omega_{kl}}^- \right). \quad (15)$$

The cross section integrated over the full 2π -range in ϕ is obtained as

$$\left\langle \frac{d\sigma}{d|t|} \right\rangle_{\Delta\Omega_l} = \sum_k \Delta\phi_k \left\langle \frac{d^2\sigma}{d|t|d\phi} \right\rangle_{\Delta\Omega_{kl}}, \quad (16)$$

with $\Delta\Omega_l = \Delta|t|_l \Delta Q^2 \Delta\nu$. Similarly, the $|t|$ -averaged cross section in the measured range is given by

$$\left\langle \frac{d^2\sigma}{d|t|d\phi} \right\rangle_{\Delta\Omega_k} = \frac{1}{\Delta|t|} \sum_l \Delta|t|_l \left\langle \frac{d^2\sigma}{d|t|d\phi} \right\rangle_{\Delta\Omega_{kl}}, \quad (17)$$

with $\Delta\Omega_k = \Delta\phi_k \Delta|t| \Delta Q^2 \Delta\nu$.

The systematic uncertainties on the extracted values of the cross section are shown in Table 2, arranged in three groups. The first group contains the systematic uncertainties on the determination of the beam flux, possible systematic effects related to the uncertainty on the energy thresholds for the detection of the low-energetic photon in the electromagnetic calorimeters, and the uncertainty on the determination of the acceptance. The second group contains the systematic uncertainties related to a variation of the energy and momentum balance of the kinematic fit, the influence of background originating from the production of ω mesons and the estimated influence of radiative corrections [25, 29]. The largest systematic effects appear in the third group, which contains the uncertainty related to the estimation of non-exclusive background as described in Sect. 4, and that related to an observed mismatch between the measured single-photon yield in the 2012 COMPASS data and a corresponding Monte Carlo simulation of the Bethe-Heitler process. The latter effect was observed in Refs. [26, 27] in a kinematic region where single-photon production is dominated by the Bethe-Heitler cross section, which is calculable at the percent level. The total systematic uncertainty Σ is obtained by quadratic summation of its components for each bin separately.

6. Results

For the background corrected final data sample the average kinematics are $\langle Q^2 \rangle = 2.0$ (GeV/c)², $\langle \nu \rangle = 12.8$ GeV, $\langle x_{Bj} \rangle = 0.093$ and $\langle -t \rangle = 0.256$ (GeV/c)². The dependences of the measured cross section on $|t|$ and ϕ are shown in Fig. 5, with the numerical values given in Table 3. The cross section in bins of $|t|$ is shown in the top panel of Fig. 5. It appears to be consistent with an exponential decrease with increasing $|t|$ for values of $|t|$ larger than about 0.25 (GeV/c)², while at smaller $|t|$ the t -dependence becomes weaker. Our result is compared to the predictions of two versions of the Goloskokov-Kroll (GK) model [15, 28].

Table 2: Summary of the estimated relative systematic uncertainties for the $|t|$ and ϕ -dependent cross sections and the integrated cross section. The values are given in percent. Note that the unidirectional uncertainty σ_{\uparrow} (σ_{\downarrow}) has to be used with positive (negative) sign.

source	σ_{\uparrow}^t	σ_{\downarrow}^t	σ_{\uparrow}^{ϕ}	$\sigma_{\downarrow}^{\phi}$	σ_{\uparrow}	σ_{\downarrow}
μ^+ flux	2	2	2	2	2	2
μ^- flux	2	2	2	2	2	2
ECal threshold	5	5	5	5	5	5
acceptance	4	7	4	7	4	7
kinem. fit	0	7	0	7	0	7
ω background	0	1	0	1	0	1
rad. corr.	2	5	2	5	2	5
μ^+ event loss	4-13	0	0-12	0-5	9	0
LEPTO norm.	5-28	3-11	5-51	3-21	8	3
Σ	12-29	10-14	12-53	12-24	14	13

The results of the GK model shown in this letter are obtained by integrating over the analysis range in the same way as it is done for the data. The dashed-dotted curve represents the cross section from the earlier version [15] as a function of $|t|$, while the upwards pointing triangles correspond to the cross section averaged over $|t|$ bins of the data. The mean cross sections for the full t -range are compared in the rightmost part of this panel. Analogously, the dotted curve and the downward pointing triangles correspond to the later version of the model [28], which was inspired by the results presented in this Letter. We observe that for the earlier version the magnitude of the predicted cross section overshoots our measurement by approximately a factor of two.

The cross section as a function of ϕ for the full measured t -range is shown in the bottom panel of Fig. 5 in eight ϕ bins of equal width. The full dots show the measured cross section for each bin and the solid curve represents the fit described below.

In order to extract the different contributions to the spin-independent cross section, a maximum-likelihood fit is applied to the data according to Eq. (4). In the fit, the measured average value of the virtual-photon polarisation parameter is used, $\epsilon = 0.996$. The ϕ -integrated cross section determined by the fit is obtained as

$$\left\langle \frac{d\sigma_T}{d|t|} + \epsilon \frac{d\sigma_L}{d|t|} \right\rangle = (8.1 \pm 0.9_{\text{stat}} \pm 1.1_{\text{sys}}) \frac{\text{nb}}{(\text{GeV}/c)^2}. \quad (18)$$

The TT and LT interference terms are obtained as

$$\left\langle \frac{d\sigma_{TT}}{d|t|} \right\rangle = (-6.0 \pm 1.3_{\text{stat}} \pm 0.7_{\text{sys}}) \frac{\text{nb}}{(\text{GeV}/c)^2} \quad (19)$$

and

$$\left\langle \frac{d\sigma_{LT}}{d|t|} \right\rangle = (1.4 \pm 0.5_{\text{stat}} \pm 0.2_{\text{sys}}) \frac{\text{nb}}{(\text{GeV}/c)^2}. \quad (20)$$

We observe a large negative contribution by σ_{TT} and a smaller positive one by σ_{LT} , which indicates a signifi-

cant role of transversely polarised photons in exclusive π^0 production.

The ϕ -dependence of the measured cross section is compared to the calculations of the GK model in the bottom panel of Fig. 5. Apart from the discrepancy in the magnitude of cross sections mentioned before, here we observe also different shapes for the measurement and the model predictions, which indicates that the relative contributions of the interference terms σ_{TT} and σ_{LT} are different when comparing measurement and model.

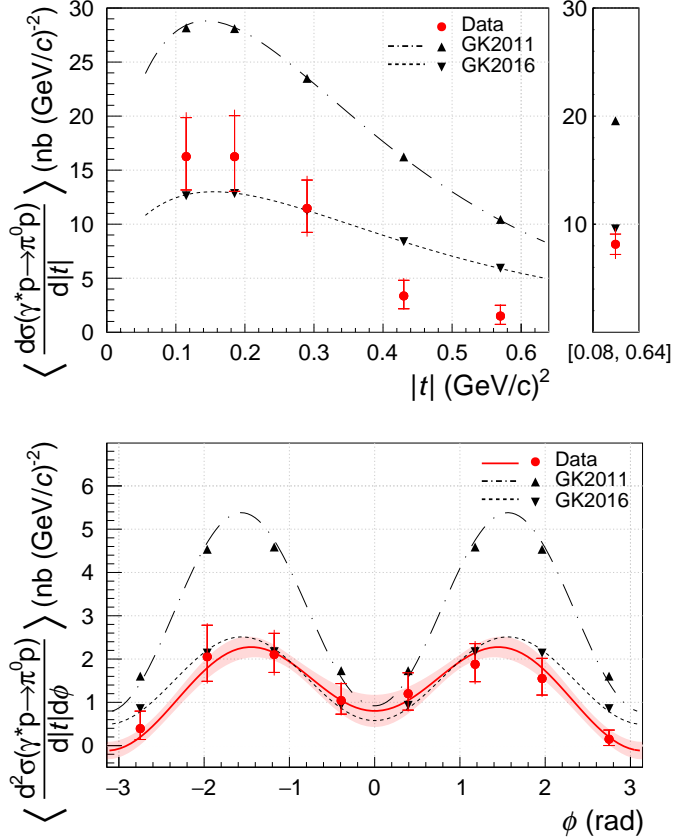


Figure 5: Average value of the differential virtual-photon proton cross section $\langle \frac{d\sigma}{d|t|} \rangle$ as a function of $|t|$ (top) and $\langle \frac{d^2\sigma}{d|t|d\phi} \rangle$ as a function of ϕ (bottom). For the top panel the data was integrated over ϕ , while for the bottom panel it was integrated over $|t|$. The result of an integration over ϕ and $|t|$ is shown in the right-most part of the top panel. Inner error bars indicate the statistical uncertainty, outer error bars the quadratic sum of statistical and systematic uncertainties. The data is compared with two predictions of the GK model [15, 28]. Radiative corrections are not applied but an estimate is included in the systematic uncertainties.

According to Refs. [10, 15], the different terms contributing to the cross section for exclusive pseudoscalar meson production, which appear in Eq. (4), depend on GPDs \tilde{H} , \tilde{E} , H_T and $\bar{E}_T = 2\tilde{H}_T + E_T$. For π^0 production a large contribution from transversely polarised virtual photons is expected, which is mainly generated by the chiral-odd GPD \bar{E}_T . It manifests itself in a large contribution from σ_{TT} and a dip in the differential cross sec-

Table 3: Numerical values of the average cross sections shown in Fig. 5.

lower ϕ bin limit	$\langle \frac{d\sigma}{d t d\phi} \rangle / \frac{\text{nb}}{(\text{GeV}/c)^2}$	lower $ t $ bin limit	$\langle \frac{d\sigma}{d t } \rangle / \frac{\text{nb}}{(\text{GeV}/c)^2}$
$-\pi$	$0.4^{+0.4}_{-0.3} _{\text{stat}}^{+0.1}_{-0.1} _{\text{sys}}$	0.08	$16.3^{+3.6}_{-3.1} _{\text{stat}}^{+2.0}_{-2.0} _{\text{sys}}$
$-\frac{3\pi}{4}$	$2.1^{+0.7}_{-0.6} _{\text{stat}}^{+0.3}_{-0.2} _{\text{sys}}$	0.15	$16.2^{+3.8}_{-3.2} _{\text{stat}}^{+2.1}_{-1.9} _{\text{sys}}$
$-\frac{\pi}{2}$	$2.1^{+0.5}_{-0.4} _{\text{stat}}^{+0.3}_{-0.3} _{\text{sys}}$	0.22	$11.5^{+2.6}_{-2.2} _{\text{stat}}^{+1.5}_{-1.4} _{\text{sys}}$
$-\frac{\pi}{4}$	$1.0^{+0.4}_{-0.3} _{\text{stat}}^{+0.2}_{-0.1} _{\text{sys}}$	0.36	$3.4^{+1.4}_{-1.2} _{\text{stat}}^{+0.8}_{-0.5} _{\text{sys}}$
0	$1.2^{+0.5}_{-0.4} _{\text{stat}}^{+0.2}_{-0.2} _{\text{sys}}$	0.5	$1.5^{+1.0}_{-0.8} _{\text{stat}}^{+0.4}_{-0.2} _{\text{sys}}$
$\frac{\pi}{4}$	$1.9^{+0.5}_{-0.4} _{\text{stat}}^{+0.2}_{-0.2} _{\text{sys}}$		
$\frac{\pi}{2}$	$1.5^{+0.5}_{-0.4} _{\text{stat}}^{+0.2}_{-0.2} _{\text{sys}}$		
$\frac{3\pi}{4}$	$0.1^{+0.2}_{-0.1} _{\text{stat}}^{+0.1}_{-0.0} _{\text{sys}}$		

tion $d\sigma/dt$ as $|t|$ decreases to zero. These features are in qualitative agreement with our results, as also with earlier measurements at different kinematics [9, 10, 13]. The COMPASS results on exclusive π^0 production provide significant constraints on modelling the chiral-odd GPDs, in particular GPD \bar{E}_T .

7. Summary and conclusion

Using exclusive π^0 muoproduction we have measured the t -dependence of the virtual-photon proton cross section for hard exclusive π^0 production at $\langle Q^2 \rangle = 2.0$ (GeV/c)², $\langle \nu \rangle = 12.8$ GeV, $\langle x_{Bj} \rangle = 0.093$ and $\langle -t \rangle = 0.256$ (GeV/c)². Fitting the azimuthal dependence reveals a large negative contribution by σ_{TT} and a smaller positive one by σ_{LT} , which indicates a significant role of transversely polarised photons in exclusive π^0 production. These results provide important input for modelling Generalised Parton Distributions. In the context of the phenomenological GK model, the statistically significant TT contribution constitutes clear experimental evidence for the existence of the chiral-odd GPD \bar{E}_T .

Acknowledgements

We thank Sergey Goloskokov and Peter Kroll for their continuous support with model predictions, Pierre Guichon for the evaluation of the Bethe-Heitler contribution taking into account the muon mass. We gratefully acknowledge the support of the CERN management and staff and the skill and effort of the technicians of our collaborating institutes.

References

References

- [1] D. Müller, D. Robaschik, B. Geyer, F.-M. Dittes and J. Hoeji, Fortsch. Phys. **42** (1994) 101.

- [2] X.-D. Ji, Phys. Rev. Lett. **78** (1997) 610.
- [3] X.-D. Ji, Phys. Rev. D **55** (1997) 7114.
- [4] A. V. Radyushkin, Phys. Lett. B **380** (1996) 417.
- [5] A. V. Radyushkin, Phys. Rev. D **56** (1997) 5524.
- [6] J. C. Collins, L. Frankfurt and M. Strikman, Phys. Rev. D **56** (1997) 2982.
- [7] A. Airapetian, et al. (HERMES Collaboration), Phys. Lett. B **659** (2008) 486.
- [8] R. de Masi, et al. (CLAS Collaboration), Phys. Rev. C **77** (2008) 042201.
- [9] I. Bedlinskiy, et al. (CLAS Collaboration), Phys. Rev. Lett **109** (2012) 112001.
- [10] I. Bedlinskiy, et al. (CLAS Collaboration), Phys. Rev. C **90** (2014) 025205.
- [11] A. Kim, et al. (CLAS Collaboration), Phys. Lett. B **768** (2017) 168.
- [12] E. Fuchey, et al. (Hall A Collaboration), Phys. Rev. C **83** (2011) 025201.
- [13] M. Defurne, et al. (Hall A Collaboration), Phys. Rev. Lett. **117** (2016) 262001.
- [14] M. Mazouz, et al. (Hall A collaboration), Phys. Rev. Lett. **118** (2017) 222002.
- [15] S. V. Goloskokov and P. Kroll, Eur. Phys. J. A **47** (2011) 112.
- [16] S. Ahmad, G. R. Goldstein and S. Liuti, Phys. Rev. D **79** (2009) 054014.
- [17] M. Göckeler, et al., Phys. Rev. Lett. **98** (2007) 222001.
- [18] P. Abbon, et al. (COMPASS Collaboration), Nucl. Instrum. Meth. A **577** (2007) 455.
- [19] P. Abbon, et al. (COMPASS Collaboration), Nucl. Instrum. Meth. A **779** (2015) 69.
- [20] F. Gautheron, et al. (COMPASS Collaboration), SPSC-P-340, CERN-SPSC-2010-014.
- [21] C. Adolph, et al. (COMPASS Collaboration), Phys. Lett. B **718** (2013) 922.
- [22] A. Sandacz and P. Sznajder, HEPGEN – generator for hard exclusive lepton production (2012), arXiv:1207.0333.
- [23] C. Regali, PhD thesis, University of Freiburg (2016), doi:10.6094/UNIFR/11449.
- [24] T. Szameitat, PhD thesis, University of Freiburg (2017), doi:10.6094/UNIFR/11686.
- [25] M. Gorzellik, PhD thesis, University of Freiburg (2018), doi:10.6094/UNIFR/15945.
- [26] P. Jörg, PhD thesis, University of Freiburg (2018), DOI:10.6094/UNIFR/12397; Exploring the size of the Proton, Springer International Publishing, doi:10.1007/978-3-319-90290-6.
- [27] R. Akhunzyanov, et al. (COMPASS Collaboration), submitted to Phys. Lett., arXiv:1802.02739.
- [28] S. V. Goloskokov and P. Kroll, private communications (2016).
- [29] A. Afanasev, I. Akushevich, V. Burkert, and K. Joo, Phys. Rev. D **66** (2002) 074004.